Supporting Information: Ab Initio Molecular Dynamics Calculations versus Quantum-State Resolved Experiments on CHD_3 + Pt(111): New Insights into a Prototypical Gas-Surface Reaction

Francesco Nattino[1], Hirokazu Ueta†[2], Helen Chadwick[2], Maarten E. van Reijzen[2], Rainer D. Beck[2], Bret Jackson[3], Marc C. van Hemert[1] and Geert-Jan Kroes[1]*

[1] Leiden Institute of Chemistry, Leiden University, Gorlaeus Laboratories, P.O. Box 9502, 2300 RA Leiden, The Netherlands.

[2] Laboratoire de Chimie Physique Moléculaire, Ecole Polytechnique Fédérale de Lausanne, Switzerland.

[3] Department of Chemistry, University of Massachusetts, Amherst, Massachusetts 01003, USA

AUTHOR INFORMATION

Present Addresses

† Hokkaido University, Sapporo 060-0819, Japan

1) EXPERIMENTAL METHODS

Quantum state resolved dissociation probabilities of CHD_3 on Pt(111) were measured in a molecular beam/surface science apparatus described previously[1-2]. Reflection absorption infrared spectroscopy (RAIRS) was used to detect the nascent dissociation products CD_3(ads) and CHD_2(ads) of CHD_3 on the cold Pt(111) surface (T_s=120 K) in order to measure both the absolute dissociation probability (S_0) and the branching ratio of the C-H and C-D cleavage channels with and without state specific laser preparation of the incident CHD_3. For the laser-off measurements above 0.7 eV incident energy, where the dissociation coefficient exceeds 1%, the King&Wells beam reflectivity technique[3] was used to measure absolute sticking coefficients of CHD_3 on Pt(111). With this method, the branching ratio could not be measured.

Molecular beam parameters are supplied in Table S1. The stream velocity (υ_0) and the width parameter (α) of the beams have been obtained by fitting a flux-weighted velocity distribution (equation (4) of Ref.[4]) to recorded TOF spectra.

2) THEORETICAL METHODS

Ab initio molecular dynamics (AIMD) calculations are performed with the VASP code[5-7]. The Pt surface is modeled with a 5 layer slab within a 3x3 supercell. A Γ-centered grid with 4x4x1 k-points samples the first Brillouin zone. Fermi smearing with a width of 0.1 eV has been used to facilitate convergence. The basis set includes plane waves up to a kinetic energy of 350 eV and core electrons have been represented with the projected augmented wave (PAW) method[8-9]. With the described computational setup, an equilibrium lattice constant of 3.975 Å has been obtained for bulk Pt, in reasonable agreement with the experimental value of 3.916 Å[10-11].

Table S2 shows the convergence of our computational setup in the evaluation of the energy barrier (E_b) for CH_4 + Pt(111). E_b is calculated as $E_{b,abs} - E_\infty$, where E_∞ is the energy of the system with the CH_4 molecule in its equilibrium geometry at large distance from the ideal metal slab and $E_{b,abs}$ is the absolute barrier energy, computed for the minimum energy transition state configuration of Ref.[12] (D1 configuration in figure 3). The calculations with a 2x2 surface unit cell show that converged results may be obtained with 5 layers. The calculations with 5 layers show that converged results may be obtained with a 3x3 surface unit cell. We estimate that, with our computational setup, the PBE value of E_b is converged to within 1 kcal/mol (43 meV).

In order to take the experimental surface temperature into account, a similar procedure as described in Ref.[13] has been followed: velocities and displacements from the equilibrium position have been assigned to surface atoms through an appropriate sampling and the optimized lattice constant has been expanded by 0.049% [10-11] in order to simulate the platinum thermal expansion from 0 to 120 K, and by 0.386% for 0 to 500 K. These configurations are used in AIMD NVE simulations (constant number of atoms N, cell volume V and total energy E) to generate surface configurations for Monte-Carlo sampling, after which the molecule-surface collisions are simulated using NVE dynamics. Sticking probabilities are based on 1000 trajectories if the computed S_0 value is included in the range $1\%<S_0<10\%$, while 2000 and 500 trajectories have been computed for the $S_0<1\%$ and the $S_0>10\%$ cases, respectively. The dissociation probability values and their error bars (95% confidence interval unless otherwise stated) are evaluated using the Wilson (or score) method[14], which has been shown to provide a reasonable estimate of confidence intervals even for extremely low probabilities (close to 0%)[15], and which yields probabilities and

standard deviations converging to the values obtained with the binomial distribution for large numbers of trajectories and probabilities.

3) AVOIDING THE PITFALLS OF THE QUASI-CLASSICAL TRAJECTORY (QCT) METHOD

a) Zero Point Energy (ZPE) Conservation Problems

Calculations for D_2 + Cu(111) show that, if motion in all molecular DOFs is modeled for average total energies of the molecule $\langle E_{tot} \rangle$ above the ZPE-corrected minimum barrier height (E_b^c), QCT calculations essentially reproduce the quantum dynamics (QD) results[16]. We therefore expect that ZPE conservation problems, which may hamper the accurate calculation of reaction probabilities near the reaction threshold if some of the coordinates are kept frozen or treated with other dynamical approximations[17-18], will not much affect the accuracy of our calculations, which are all done for $\langle E_{tot} \rangle$ well above E_b^c (Table 1 of the paper).

To make sure that ZPE conservation problems have no significant effect on our calculations, we looked at whether evidence of ZPE violation could be found in our actual AIMD calculations. No strong proof of ZPE violation has been found in the dynamics as a possible reason of the too high reaction probability even at low average incidence energy $\langle E_i \rangle$: the available energy to the reaction (the sampled E_{tot}) is larger than the ZPE-corrected minimum energy barrier from static calculations, in almost all (i.e., 143) of the 144 reacted trajectories computed in total for the three lowest $\langle E_i \rangle$ laser-off simulations, and in all of the laser-on reacted trajectories. Furthermore, the reaction probability is overestimated even at the highest $\langle E_i \rangle$, where the experimental reaction probabilities are larger than 15% and ZPE violation is not expected to play a role.

b) Artificial intramolecular vibrational energy redistribution (IVR)

In order to avoid the potential problem of artificial energy flow among vibrations alluded to above, we focus on two types of experiment. The first ("laser-off") experiment addresses the reactivity of CHD_3 in a hyperthermal supersonic beam, in which the vibrational ground state has the highest population. In the second type of experiment the ν_1 CH-stretch is pre-excited with one quantum but due to the localization of the vibrational mode on the CH bond, this mode is off-resonance with other vibrations, so that artificial intra-molecular vibrational energy redistribution (IVR) is minimised[19]. We carefully verified that AIMD is able to simulate freely vibrating CH-stretch (ν_1) excited CHD_3 without significant energy 'leakage' from the ν_1 mode to others. **Figure S1** shows the normal mode energies as a function of time, averaged over 100 trajectories for which the initial conditions (normal mode vibrational coordinates and velocities) sample classical microcanonical distributions. The normal mode energies have been evaluated by projecting the vibrational coordinates of CHD_3 onto its equilibrium normal mode coordinates. As evident from **Figure S1**, the vibrational energy imparted to the ν_1 mode remains localized in this vibrational mode on the time-scale of the collisions in our simulations (100-200 fs).

c) Role of Tunneling

Early on, it was argued that an exponential dependence of the dissociation probability on E_i observed in supersonic molecular beam experiments between E_i = 0.70 to 0.98 eV should be due to tunneling, on the basis of a one-dimensional model[20]. However, this model implied a very high ZPE-corrected barrier height of 1.25 eV, whereas experiments suggest a value of only 0.6 ± 0.2 eV[21].

Even though we use it here for a different surface (Ni(100)), the reaction path Hamiltonian model described in Ref.[22] allows an estimate to be made of the tunneling contribution for the lowest surface temperature (T_s) considered in our calculations on CHD_3+Pt(111). The reaction probability has been computed by averaging the results of one-dimensional (1D) quantum dynamics calculations over surface sites and a surface atom coordinate, after setting all the vibrationally non-adiabatic couplings to zero (see figure 9 and the corresponding more detailed discussion in Ref.[22]). The tunneling contribution can be excluded by setting all the 1D reaction probabilities ≤ 0.5 equal to zero. The reaction probability curves including and excluding tunneling contributions are plotted in **Figure S2**. The two curves are displaced from one another along the energy axis by less than 1 kJ/mol (0.01 eV) when $S_0 = 10^{-3}$ for T_s = 120 K.

Since we only simulate conditions for which the experimental reaction probabilities are > 0.01, we do not expect that the neglect of tunneling effects in our calculations has a large effect on our most important conclusions. In particular, the neglect of tunneling should hardly affect our conclusion regarding the barrier height for CHD_3 + Pt(111), the conclusion being that the PBE functional underestimates this quantity by 0.1 eV. This does not mean that tunneling does not influence the reaction: at the incidence energy where the quantum mechanical reaction probability is 0.01 (80.5 kJ/mol ≈ 0.83 eV), the tunneling contribution to the reaction is approximately 10% (i.e., the tunneling contribution to the reaction probability is approximately 0.001). The reason that the tunneling contribution is so low for this low incidence energy (for Ni(100) the zero-point energy corrected barrier height for the static surface is 0.78 eV[12]) is that even at T_s=120 K excited surface vibrational states are populated, and this allows reaction through a classical over the barrier mechanism because the outward motion of the surface atom above which methane reacts lowers the reaction barrier[12].

The comparison of calculations on reaction of a supersonic beam of CH_4 with Pt(111) at E_i = 0.62 eV and T_S = 200 K[23], which used a statistical model and either included[21] or excluded[24] the effect of tunneling, likewise suggests only a minor role for tunneling under the conditions addressed by us.

Finally, we also expect no problems due to neglect of tunneling with computing branching ratios for CHD_3 dissociation into CD_3 + H and CHD_2 + D, as a recent QCT study was able to show that the strong kinetic isotope effect observed previously when comparing CH_4 to CD_4 dissociation on Pt(111)[25] could be explained on the basis of the molecules' different ZPEs[26].

4) EFFECT OF VIBRATIONALLY EXCITED STATES ON LASER-OFF REACTIVITY

We analyzed the contribution of thermally excited vibrational states to the theoretical laser-off reactivity (Table S3). At the lowest E_i, the vibrationally excited molecules are 2.5 times more reactive than the ground state ones; this factor decreases with increasing E_i. At the highest simulated E_i (1.53 eV), the reactivity of ground-state molecules is roughly equal to that of the vibrationally excited molecules. The larger effect of vibration at low E_i arises because at low E_i vibrational energy is needed to overcome the barrier for dissociation, whereas at higher E_i molecules already possess enough translational energy to dissociate.

5) EFFECT OF SURFACE MOTION ON REACTION

In a similar analysis as used in earlier work that only allowed one-dimensional motion of a single surface atom[27], we looked at the time evolution of the vertical displacement of the surface atom closest to the incident molecule (**Figure S3**). Recoil

is observed if the average is performed over scattered trajectories at all E_i, but for reactive trajectories recoil is only seen at high E_i. The profile for reactive trajectories at low E_i is different: reaction occurs only if the closest surface atom is above the surface plane and moves towards the projectile, thereby lowering the barrier and increasing the relative velocity. At higher E_i reaction occurs regardless of the surface atom behavior, and only recoil is seen[27]. Our AIMD results confirm the validity of the same result obtained earlier with models using a much more simplified treatment of surface motion[27-30].

Supporting Tables

Translational Energy (eV)	Total Energy (eV)	State	Set Nozzle Temperature (K)	Gas Temperature (K)	v_0 (m/s)	α (m/s)
0.514	0.552	Laser-off	500	534	2263	156
0.727	0.837	Laser-off	700	764	2679	227
0.781	**0.919**	**Laser-off**	**750**	**836**	**2774**	**248**
0.830	**0.997**	**Laser-off**	**800**	**902**	**2857**	**265**
0.875	**1.074**	**Laser-off**	**850**	**971**	**2926**	**291**
1.376	**1.487**	**Laser-off**	**700**	**768**	**3739**	**417**
1.535	**1.7016**	**Laser-off**	**800**	**901**	**3948**	**482**
0.276	0.648	ν_1=1	-	300	1662	98
0.397	**0.769**	**ν_1=1**	**400**	**412**	**1992**	**122**
0.514	**0.886**	**ν_1=1**	**500**	**534**	**2263**	**156**

Table S1. Molecular beam parameters. v_0 and α represent the stream velocity and the width parameter of the beams, respectively. The beams which have been simulated using AIMD have been highlighted.

Surface Unit Cell Size	Number of Atomic Layers	k-point grid	Cut-off energy (eV)	E_b (eV)
2x2	4	8x8x1	350	0.926
2x2	4	8x8x1	400	0.931
2x2	4	8x8x1	600	0.933
2x2	4	16x16x1	350	0.928
2x2	5	8x8x1	350	0.872
2x2	10	8x8x1	350	0.885
3x3	4	6x6x1	350	0.887
3x3	**5**	**4x4x1**	**350**	**0.805**
3x3	5	4x4x1	500	0.811
3x3	5	8x8x1	350	0.813
4x4	4	4x4x1	350	0.861
4x4	5	4x4x1	500	0.801

Table S2. Convergence tests of the electronic structure calculations for CH_4 + Pt(111). The barrier energy E_b has been computed varying the surface unit cell size, the number of atomic layers in the slab, the k-point grid size (Γ-point is always included) and the cut-off energy for the plane waves expansion. The energy barrier of our computational setup has been highlighted.

$\langle E_i \rangle$ (eV)	T_S (K)	T_{Gas} (K)	$P(\mathrm{v}=0)$	$S_0^{\mathrm{v}=0}$	$S_0^{\mathrm{v}\neq0}$	$S_0^{\mathrm{v}\neq0}/S_0^{\mathrm{v}=0}$
0.78	120	836	42.4%	(1.8 ± 0.6) %	(4.4 ± 0.9) %	2.4
0.83	120	902	37.6%	(3.3 ± 0.9) %	(6.6 ± 1.0) %	2.0
0.87	120	971	29.4%	(3.9 ± 1.1) %	(6.9 ± 1.0) %	1.8
1.38	500	768	47.2 %	(34.3 ± 3.1) %	(48.5 ± 3.1) %	1.4
1.53	500	901	38.8 %	(49.5 ± 3.6) %	(50.0 ± 2.9) %	1

Table S3. Population and computed reactivity of ground state and vibrationally excited molecules in the laser-off simulations. $\langle E_i \rangle$ is the average translational energy, T_S is the surface temperature, T_{Gas} is the gas temperature in the expansion nozzle, $P(\mathrm{v}=0)$ is the v = 0 population and $S_0^{\mathrm{v}=0}$ ($S_0^{\mathrm{v}\neq0}$) is the dissociation probability of the ground state (vibrationally excited) molecules in the thermally excited beams. Error bars represent 68.3 % confidence intervals.

Supporting Figures

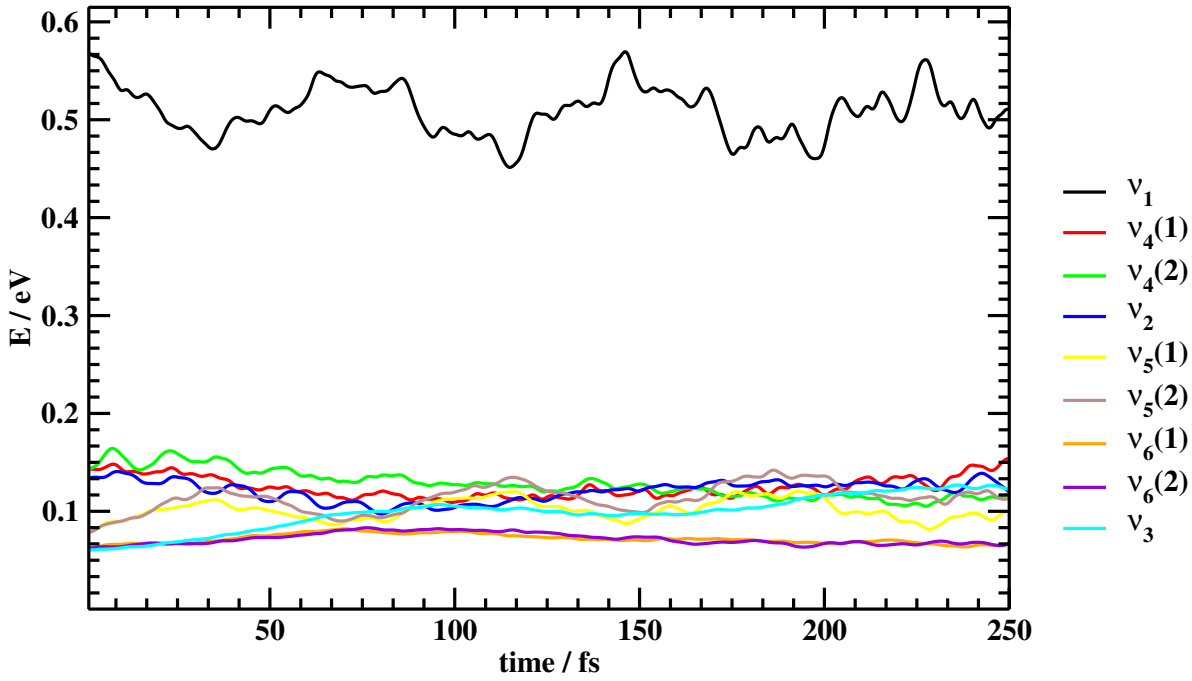

Figure S1. The normal mode energies are plotted as a function of time for freely vibrating CH-stretch (ν_1, in black) excited CHD_3. The energies plotted here are the result of an average over 100 trajectories.

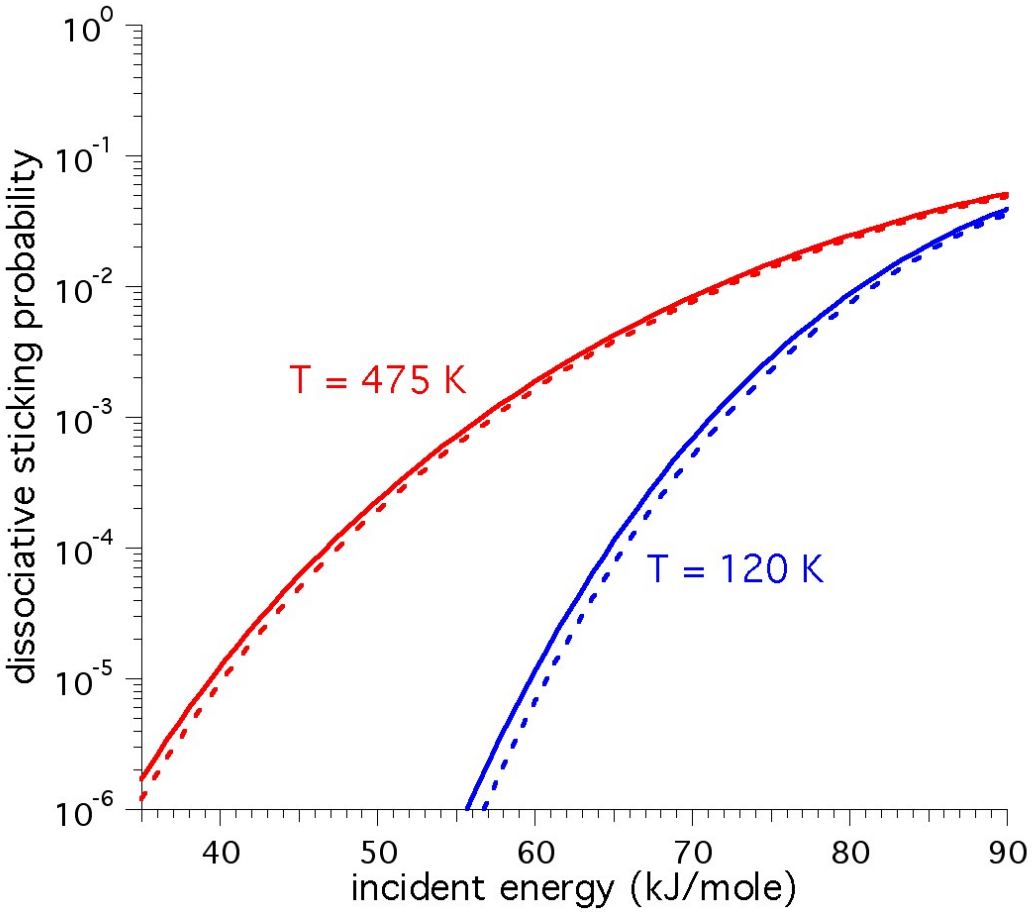

Figure S2. Dissociative sticking probability as a function of incident energy for vibrationally ground state CH_4 incident on Ni(100) at the temperatures indicated. The curves are from the reaction path model described in Ref.[22], for the case where the vibrationally non-adiabatic couplings are set equal to zero. The dashed lines exclude contributions to the sticking from tunneling. The results reported for T_s = 475 K are from Ref.[22].

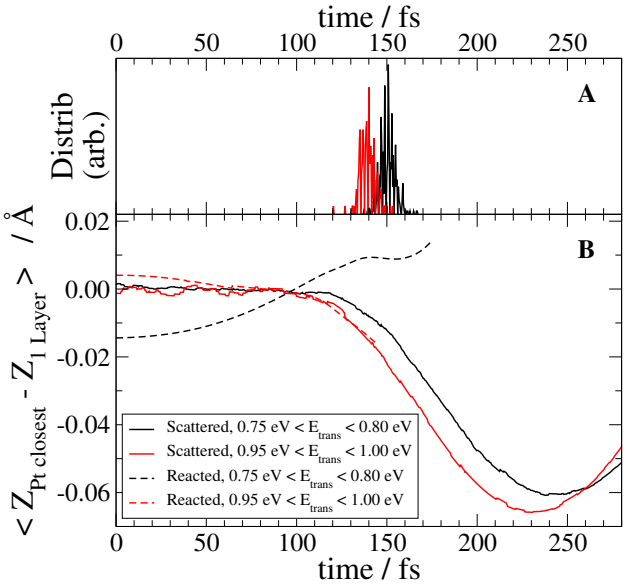

Figure S3. (A): Arrival distributions at the inner turning point in Z for scattered molecules for 0.75 eV < E_i < 0.80 eV (black) and for 0.95 eV < E_i < 1.00 eV (red). (B): Vertical displacement of the closest first layer atom as a function of time, averaged over scattered (solid lines) and reacted (dashed lines) laser-off trajectories in the two ranges of E_i (black and red, as in panel A).

References

(1) Chen, L.; Ueta, H.; Bisson, R.; Beck, R. D. Quantum State-Resolved Gas/Surface Reaction Dynamics Probed by Reflection Absorption Infrared Spectroscopy. *Rev. Sci. Instrum.* **2013,** *84*, 053902.

(2) Ueta, H.; Chen, L.; Beck, R. D.; Colon-Diaz, I.; Jackson, B. Quantum State-Resolved CH_4 Dissociation on Pt(111): Coverage Dependent Barrier Heights from Experiment and Density Functional Theory. *Phys. Chem. Chem. Phys.* **2013,** *15*, 20526-20535.

(3) King, D. A.; Wells, M. G. Reaction-Mechanism in Chemisorption Kinetics - Nitrogen on (100) Plane of Tungsten. *Proc. R. Soc. Lond. A-Math. Phys. Sci.* **1974,** *339*, 245-269.

(4) Michelsen, H. A.; Auerbach, D. J. A Critical-Examination of Data on the Dissociative Adsorption and Associative Desorption of Hydrogen at Copper Surfaces. *J. Chem. Phys.* **1991,** *94*, 7502-7520.

(5) Kresse, G.; Furthmüller, J. Efficient Iterative Schemes for Ab Initio Total-Energy Calculations Using a Plane-Wave Basis Set. *Phys. Rev. B* **1996,** *54*, 11169-11186.

(6) Kresse, G.; Hafner, J. Ab-Initio Molecular-Dynamics for Liquid-Metals. *Phys. Rev. B* **1993,** *47*, 558-561.

(7) Kresse, G.; Hafner, J. Ab-Initio Molecular-Dynamics Simulation of the Liquid-Metal Amorphous-Semiconductor Transition in Germanium. *Phys. Rev. B* **1994,** *49*, 14251-14269.

(8) Kresse, G.; Joubert, D. From Ultrasoft Pseudopotentials to the Projector Augmented-Wave Method. *Phys. Rev. B* **1999,** *59*, 1758-1775.

(9) Blochl, P. E. Projector Augmented-Wave Method. *Phys. Rev. B* **1994,** *50*, 17953-17979.

(10) Arblaster, J. W. Crystallographic Properties of Platinum. *Platinum Met. Rev.* **1997,** *41*, 12-21.

(11) Arblaster, J. W. Crystallographic Properties of Platinum New Methodology and Erratum. *Platinum Met. Rev.* **2006,** *50*, 118-119.

(12) Nave, S.; Tiwari, A. K.; Jackson, B. Methane Dissociation and Adsorption on Ni(111), Pt(111), Ni(100), Pt(100), and Pt(110)-(1×2): Energetic Study. *J. Chem. Phys.* **2010,** *132*, 054705.

(13) Nattino, F.; Díaz, C.; Jackson, B.; Kroes, G. J. Effect of Surface Motion on the Rotational Quadrupole Alignment Parameter of D_2 Reacting on Cu(111). *Phys. Rev. Lett.* **2012,** *108*, 236104.

(14) Wilson, E. B. Probable Inference, the Law of Succession, and Statistical Inference. *J. Am. Stat. Assoc.* **1927,** *22*, 209-212.

(15) Agresti, A.; Coull, B. A. Approximate Is Better Than "Exact" for Interval Estimation of Binomial Proportions. *Am. Stat.* **1998,** *52*, 119-126.

(16) Díaz, C.; Olsen, R. A.; Auerbach, D. J.; Kroes, G. J. Six-Dimensional Dynamics Study of Reactive and Non Reactive Scattering of H_2 from Cu(111) Using a Chemically Accurate Potential Energy Surface. *Phys. Chem. Chem. Phys.* **2010,** *12*, 6499-6519.

(17) Darling, G. R.; Wang, Z. S.; Holloway, S. Exploring the Applicability of Classical Mechanics in H_2 Scattering and Reaction at Metal Surfaces. *Phys. Chem. Chem. Phys.* **2000,** *2*, 911-917.

(18) Mastromatteo, M.; Jackson, B. The Dissociative Chemisorption of Methane on Ni(100) and Ni(111): Classical and Quantum Studies Based on the Reaction Path Hamiltonian. *J. Chem. Phys.* **2013,** *139*, 194701.
(19) Xie, Z.; Bowman, J. M.; Zhang, X. Quasiclassical Trajectory Study of the Reaction $H+CH_4(\nu_3=0,1)\rightarrow CH_3+H_2$ Using a New Ab Initio Potential Energy Surface. *J. Chem. Phys.* **2006,** *125*, 133120.
(20) Schoofs, G. R.; Arumainatagam, C. R.; Master, M. C.; Madix, R. J. Dissociative Chemisorption of Methane on Pt(111). *Surf. Sci.* **1989,** *215*, 1-28.
(21) Donald, S. B.; Navin, J. K.; Harrison, I. Methane Dissociative Chemisorption and Detailed Balance on Pt(111): Dynamical Constraints and the Modest Influence of Tunneling. *J. Chem. Phys.* **2013,** *139*, 214707.
(22) Jackson, B.; Nave, S. The Dissociative Chemisorption of Methane on Ni(100): Reaction Path Description of Mode-Selective Chemistry. *J. Chem. Phys.* **2011,** *135*, 114701.
(23) Harris, J.; Simon, J.; Luntz, A. C.; Mullins, C. B.; Rettner, C. T. Thermally Assisted Tunneling - CH_4 Dissociation on Pt(111). *Phys. Rev. Lett.* **1991,** *67*, 652-655.
(24) Donald, S. B.; Harrison, I. Dynamically Biased Rrkm Model of Activated Gas-Surface Reactivity: Vibrational Efficacy and Rotation as a Spectator in the Dissociative Chemisorption of CH_4 on Pt(111). *Phys. Chem. Chem. Phys.* **2012,** *14*, 1784-1795.
(25) Luntz, A. C.; Bethune, D. S. Activation of Methane Dissociation on a Pt(111) Surface. *J. Chem. Phys.* **1989,** *90*, 1274-1280.
(26) Shen, X. J.; Lozano, A.; Dong, W.; Busnengo, H. F.; Yan, X. H. Towards Bond Selective Chemistry from First Principles: Methane on Metal Surfaces. *Phys. Rev. Lett.* **2014,** *112*, 046101.
(27) Tiwari, A. K.; Nave, S.; Jackson, B. The Temperature Dependence of Methane Dissociation on Ni(111) and Pt(111): Mixed Quantum-Classical Studies of the Lattice Response. *J. Chem. Phys.* **2010,** *132*, 134702.
(28) Jackson, B.; Nave, S. The Dissociative Chemisorption of Methane on Ni(111): The Effects of Molecular Vibration and Lattice Motion. *J. Chem. Phys.* **2013,** *138*, 174705.
(29) Nave, S.; Jackson, B. Methane Dissociation on Ni(111): The Effects of Lattice Motion and Relaxation on Reactivity. *J. Chem. Phys.* **2007,** *127*, 224702.
(30) Nave, S.; Jackson, B. Methane Dissociation on Ni(111): The Role of Lattice Reconstruction. *Phys. Rev. Lett.* **2007,** *98*, 173003.